Computer tutorial N°3

Goal-oriented error estimation and mesh adaptivity

Goal functional, primal problem, adjoint problem, goal-oriented a posteriori error estimate, mesh adaptivity

We consider a similar setup as in tutorials N°1 and N°2, where $\Omega \subset \mathbb{R}^2$ is an open, bounded, and connected set with a polygonal and Lipschitz boundary $\partial\Omega = \Gamma_{\rm D} \cup \Gamma_{\rm N}$. In the first part of the exercice, Ω is the unit square $\Omega =]0,1[\times]0,1[$, see Figure 1. The prescribed loading is as follows: Neumann boundary conditions with unit normal flux are applied on the top side $\Gamma_N \subset \partial\Omega$ of the square; homogeneous Dirichlet conditions are applied on the complementary part $\Gamma_D \subset \partial\Omega$ made of the 3 other sides; there is no source term in Ω.

The model problem thus reads: find $u : \Omega \to \mathbb{R}$ such that

$$-\Delta u = 0 \qquad \text{in } \Omega, \tag{1a}$$
$$u = 0 \qquad \text{on } \Gamma_{\rm D}, \tag{1b}$$
$$-\nabla u \cdot \boldsymbol{n}_\Omega = -1 \qquad \text{on } \Gamma_{\rm N}. \tag{1c}$$

The quantity $\boldsymbol{\sigma} := -\nabla u$ is the flux associated to u. The problem has an analytical (smooth) solution, given by

$$u(x,y) = 2\sum_{k=1}^{\infty}(1-(-1)^k)\frac{\sin(k\pi x)\sinh(k\pi y)}{(k\pi)^2\cosh(k\pi)}. \tag{2}$$

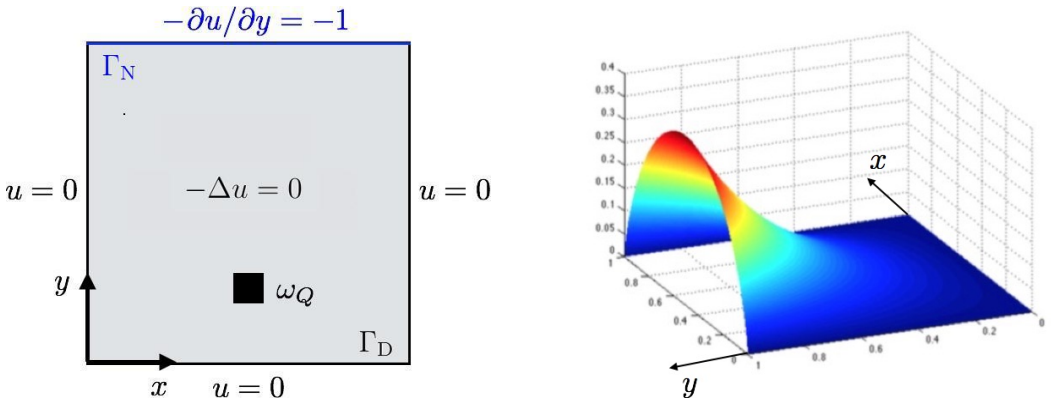

Figure 1: Reference problem and plot of the exact solution

We define the two quantities of interest:

$$Q_1(u) := \frac{1}{|\omega_Q|}\int_{\omega_Q} u \quad \text{and} \quad Q_2(u) := -\frac{1}{|\Gamma_{\rm R}|}\int_{\Gamma_{\rm R}} \frac{\partial u}{\partial x}, \tag{3}$$

where Q_1 corresponds to the average of u in the subregion $\omega_Q := (0.45, 0.55) \times (0.2, 0.3)$, and Q_2 is the average of the normal flux on the right-hand edge $\Gamma_{\rm R}$ at $x = 1$. The error

estimation by flux equilibration developed in the previous computer tutorials N°1 and N°2 will be reused in the following.

Denoting $V := \{v \in H^1(\Omega) : v|_{\Gamma_D} = 0\}$, the primal problem reads as: find $u \in V$ such that for all $v \in V$,

$$(\nabla u, \nabla v) = \langle v, 1\rangle_{\Gamma_N}. \tag{4}$$

Let $\mathcal{T}_\ell$ be a triangulation of Ω. The finite element method seeks for an approximate solution u_ℓ to the exact solution u in the discrete piecewise polynomial subspace of V

$$V_\ell^p := \{v_\ell \in V, v_\ell|_K \in \mathcal{P}_p(K) \quad \forall K \in \mathcal{T}_\ell\} = \mathcal{P}_p(\mathcal{T}_\ell) \cap V, \tag{5}$$

where the polynomial degree $p \geq 1$; $u_\ell \in V_\ell^p$ is such that for all $v_\ell \in V_\ell^p$,

$$(\nabla u_\ell, \nabla v_\ell) = \langle v_\ell, 1\rangle_{\Gamma_N}. \tag{6}$$

Above, $\mathcal{P}_q(K)$ stands for the space of polynomials of total degree at most $q \geq 0$ on the mesh element $K \in \mathcal{T}_\ell$ and $\mathcal{P}_q(\mathcal{T}_\ell)$ denotes piecewise q-degree polynomials with respect to the mesh $\mathcal{T}_\ell$.

Exercise 1. (Analysis of the error)

1. Generate a triangular mesh $\mathcal{T}_0$ of Ω with `int nds = 10` subdivisions in each direction (similar mesh as in tutorial N°1). For the quantity of interest Q_1, it may be convenient to respect the subregion ω_Q, which can in FreeFem++ be achieved using the command `buildmesh`. For Q_2, the meshes created by the command `Th = square(nds,nds)` appear less sensitive to the approximation of the exact solution u described in item 3 below. Successive meshes will in this exercise be obtained using the command `Th=splitmesh(Th,2)` for uniform mesh refinement.

2. Perform the assembly of problem (6), in order to compute the approximate solution u_ℓ in V_ℓ^p, starting with $\ell = 0$. We first consider `Pcont P1`.

3. Obtain an approximation of the exact solution u given by (2) together with its derivatives by relying on `int uExpres = 50` first terms from the development (2). More precisely, we interpolate u in a finer space than V_ℓ^p, using a) a refined mesh of $\mathcal{T}_\ell$ obtained by `int noverkill = 2` uniform refinements of $\mathcal{T}_\ell$ and b) using a higher polynomial degree `Pcontpp P2`.

4. Plot the exact solution u and its finite element approximation u_ℓ.

5. Using the sequence $\mathcal{T}_\ell$ of uniformly refined meshes, plot the convergence of the global discretization error in the energy norm $\|\nabla(u - u_\ell)\|$, as well as that of the error $|Q_j(u) - Q_j(u_\ell)|$ in both quantities of interest Q_1 and Q_2. Comment on the obtained results.

Answer 1. (Analysis of the error)

The answers to items 1–3 are contained in the script `TP3.edp`. We now illustrate answers to questions 4–5.

4. One should obtain the results as in Figure 2.

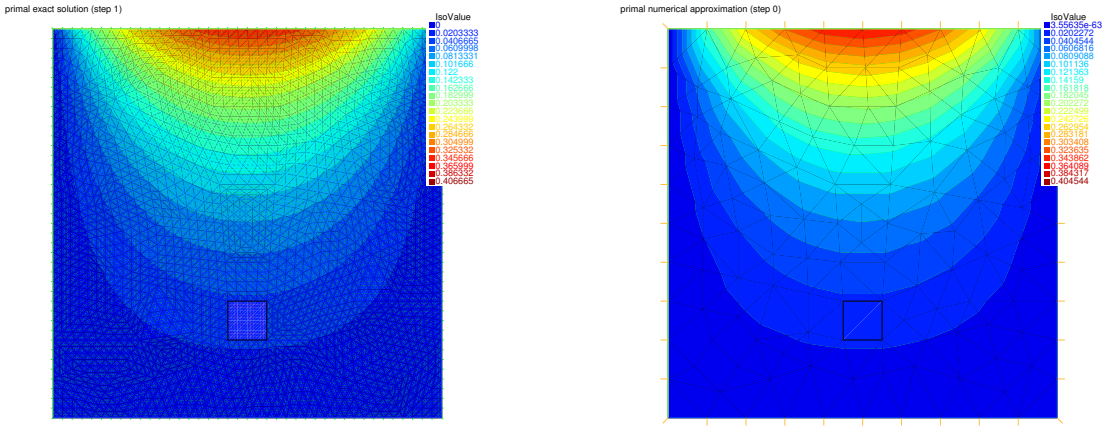

Figure 2: Exact solution u (left) and approximate solution u_ℓ (right, $p = 1$)

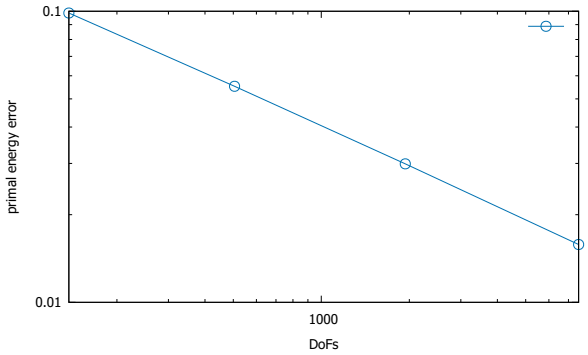

Figure 3: Energy error $\|\nabla(u - u_\ell)\|$ with respect to the DoFs, $p = 1$

5. One should obtain the results as in Figures 3 and 4. In a smooth case, the energy error converges as $\mathcal{O}(\text{DoFs})^{-p/2}$, whereas the error in the goal functional as $\mathcal{O}(\text{DoFs})^{-p}$. As the solution u of (2) is smooth, we indeed observe the $\mathcal{O}(\text{DoFs})^{-1/2}$ rate for the energy error, since we illustrate here the polynomial degree $p = 1$. As for the goal functional Q_1 from (3), the convergence rate is indeed doubled to $\mathcal{O}(\text{DoFs})^{-1}$. This is, however, not the case for Q_2, which is connected with its non-volumetric nature: we only have $\mathcal{O}(\text{DoFs})^{-1/2}$ rate for Q_2.

Exercise 2. (Goal-oriented error estimation)

For both $j \in \{1, 2\}$, we would be tempted to define the adjoint problems as: find $\tilde{u} \in V$ such that for all $v \in V$,

$$(\nabla\tilde{u}, \nabla v) = Q_j(v). \tag{7}$$

This is perfectly fine for the volumetric quantity of interest Q_1 from (3), where the strong form of the problem reads: find $\tilde{u} : \Omega \to \mathbb{R}$ such that

$$-\Delta\tilde{u} = \tilde{f} \qquad \text{in } \Omega, \tag{8a}$$
$$u = 0 \qquad \text{on } \Gamma_\text{D}, \tag{8b}$$
$$-\nabla\tilde{u}\cdot\boldsymbol{n}_\Omega = 0 \qquad \text{on } \Gamma_\text{N} \tag{8c}$$

with the source term

$$\tilde{f} := \frac{1}{|\omega_Q|} 1_{\omega_Q}$$

only nonzero in the subregion ω_Q.

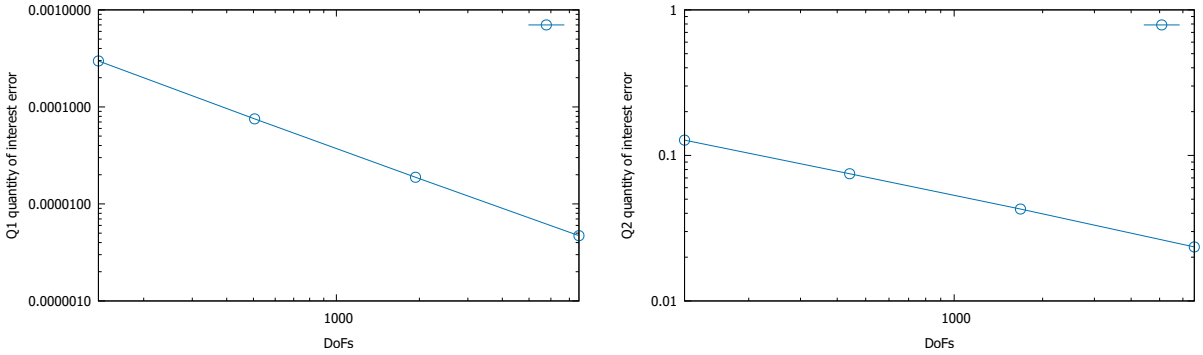

Figure 4: Error in the quantity of interest $|Q_j(u) - Q_j(u_\ell)|$ in function of the DoFs, $p = 1$ (left for Q_1, right for Q_2)

On the other hand, for the quantity of interest Q_2 from (3) of surface nature, $Q_2(v)$ is not even defined for $v \in V$ (indeed, the trace of $\frac{\partial v}{\partial x}$ on Γ_{R} does not necessarily exist). In this case, actually, proceeding as in, e.g., [1], the correct form of the adjoint problems reads: find $\tilde{u} \in H^1(\Omega)$ such that $\tilde{u}|_{\Gamma_{\mathrm{D}}} = \tilde{u}_{\mathrm{D}}$ and such that for all $v \in V$,

$$(\nabla \tilde{u}, \nabla v) = 0. \tag{9}$$

The strong form of (9) is then: find $\tilde{u} : \Omega \to \mathbb{R}$ such that

$$-\Delta \tilde{u} = 0 \qquad \text{in } \Omega, \tag{10a}$$
$$u = \tilde{u}_{\mathrm{D}} \qquad \text{on } \Gamma_{\mathrm{D}}, \tag{10b}$$
$$-\nabla \tilde{u} \cdot \boldsymbol{n}_\Omega = 0 \qquad \text{on } \Gamma_{\mathrm{N}}. \tag{10c}$$

Here $\tilde{u}_{\mathrm{D}}$ is the "extractor function" which needs to take the value $\frac{1}{|\Gamma_{\mathrm{R}}|} = 1$ on Γ_{R} and should "vanish" on the rest of Γ_{D}. In order to correctly use it in (10b), we, however, need it in the space $H^{1/2}(\Gamma_{\mathrm{D}})$, i.e., it has to be a trace of a function from $H^1(\Omega)$. This means that we actually cannot set $\tilde{u}_{\mathrm{D}}$ to zero in the rest of the Dirichlet boundary Γ_{D}. In our problem, where, on the bottom side of the square $y = 0$, the exact solution u is zero and also its gradient is small, the value of $\tilde{u}_{\mathrm{D}}$ on $y = 0$ actually does not count much. Consequently, we set $\tilde{u}_{\mathrm{D}} = x$ on the bottom side $y = 0$ and $\tilde{u}_{\mathrm{D}} = 0$ on the left side $x = 0$ (this is done in the script below `VthP1 ValDir`). As usual, we also introduce the adjoint flux $\tilde{\boldsymbol{\sigma}} := -\nabla \tilde{u}$.

1. Perform the assembly of problem (7) for Q_1 and (9) for Q_2, in order to compute approximate solutions $\tilde{u}_\ell$ with FEM and the same initial mesh as for the primal problem, and plot them. What is the physical representation of the adjoint loading?

2. Construct the equilibrated fluxes: $\boldsymbol{\sigma}_\ell$ for the primal problem and $\tilde{\boldsymbol{\sigma}}_\ell$ for the two adjoint problems. Attention, for the original (primal) problem (1), we now have an inhomogeneous Neumann boundary condition imposed on Γ_{N}, so that the boundary conditions of the patch mixed finite element minimizations need to be appropriately adjusted for boundary vertices lying at Γ_{N}.

3. Considering again the same meshes for primal and adjoint problems, compute the following basic error estimate for the first quantity of interest Q_1:

$$|Q_1(u) - Q_1(u_\ell)| = |(\nabla(u - u_\ell), \nabla(\tilde{u} - \tilde{u}_\ell))| \leq \eta_{\mathrm{QI}} := \eta_\ell \tilde{\eta}_\ell, \tag{11}$$

where η_ℓ and $\tilde{\eta}_\ell$ are the equilibrated fluxes estimators for primal and adjoint problems,

$$\|\nabla(u-u_\ell)\| \le \eta_\ell := \|\boldsymbol{\sigma}_\ell + \nabla u_\ell\| \quad \text{and} \quad \|\nabla(\tilde{u}-\tilde{u}_\ell)\| \le \tilde{\eta}_\ell := \|\tilde{\boldsymbol{\sigma}}_\ell + \nabla \tilde{u}_\ell\|. \tag{12}$$

We remark that there are no data oscillation estimators here. For the second quantity of interest Q_2, the situation is a bit more involved. Following again [1], equation (4.14) (take $s_h^i = u_h^i = u_\ell$), we, however, have (after integration by parts)

$$|Q_2(u) - Q_2(u_\ell)| \le \eta_{\mathrm{QI}} := \eta_\ell \tilde{\eta}_\ell + |\langle \nabla u_\ell \cdot \boldsymbol{n}_\Omega, \tilde{u}_{\mathrm{D}} \rangle_{\Gamma_{\mathrm{D}}} - \langle \boldsymbol{\sigma}_\ell \cdot \boldsymbol{n}_\Omega, \tilde{u}_\ell \rangle_{\Gamma_{\mathrm{N}}}|. \tag{13}$$

Note there are two supplementary boundary terms in comparison with (11).

4. Analyze the evolution of the goal estimate η_{QI} with respect to the exact goal error $|Q_j(u) - Q_j(u_\ell)|$, $j = 1, 2$, for the sequence of uniformly refined meshes performed in Exercice 1. In particular, plot the effectivity indices given by

$$\frac{\eta_{\mathrm{QI}}}{|Q_j(u) - Q_j(u_\ell)|}, \tag{14}$$

as well as the effectivity indices related to the primal and dual energy estimates (12)

$$\frac{\eta_\ell}{\|\nabla(u-u_\ell)\|} \quad \text{and} \quad \frac{\tilde{\eta}_\ell}{\|\nabla(\tilde{u}-\tilde{u}_\ell)\|}. \tag{15}$$

5. For both cases $j \in \{1, 2\}$, implement the improved bound

$$|Q_j(u) - Q_j(u_\ell) - C_\ell| \le \frac{1}{2}\eta_\ell \tilde{\eta}_\ell + |\langle (\nabla u_\ell + \boldsymbol{\sigma}_\ell) \cdot \boldsymbol{n}_\Omega, \tilde{u}_{\mathrm{D}} \rangle_{\Gamma_{\mathrm{D}}}|, \tag{16}$$

where $C_\ell := \frac{1}{2}(\boldsymbol{\sigma}_\ell + \nabla u_\ell, \tilde{\boldsymbol{\sigma}}_\ell + \nabla \tilde{u}_\ell)$ is a computable correction term and where $\tilde{u}_{\mathrm{D}} = 0$ for Q_1 (see [1, Theorem 4.8] for the boundary term appearing for Q_2). This bound can be rewritten as

$$|Q_j(u) - Q_j(u_\ell)| \le \eta_{\mathrm{QI}}^{\mathrm{impr}} := \max_{\theta=\pm 1} \Big| C_\ell + \theta \Big(\frac{1}{2}\eta_\ell \tilde{\eta}_\ell + |\langle (\nabla u_\ell + \boldsymbol{\sigma}_\ell) \cdot \boldsymbol{n}_\Omega, \tilde{u}_{\mathrm{D}} \rangle_{\Gamma_{\mathrm{D}}}| \Big) \Big|. \tag{17}$$

6. In a similar way as in question 4. of Exercise 2, analyze the evolution of the new goal estimate with respect to the exact goal error.

Answer 2. (Goal-oriented error estimation)

The answers to items 3 and 5 are contained in the script `TP3.edp`. As for the other questions:

1. One should obtain the results as in Figure 5. We note a strong localization of the dual approximation $\tilde{u}_\ell$ around the subregion ω_Q for the quantity of interest Q_1. For Q_2, it follows from our choice of the extractor function $\tilde{u}_{\mathrm{D}}$ in (9)–(10) that

$$\tilde{u}(x, y) = \tilde{u}_\ell(x, y) = x. \tag{18}$$

The physical representation of the adjoint loading is a volumetric source term with value $1/|\omega_Q|$ in ω_Q for Q_1 and imposition of the Dirichlet boundary condition equal to the extractor function $\tilde{u}_{\mathrm{D}}$ with value $1/|\Gamma_{\mathrm{R}}|$ on Γ_{R}.

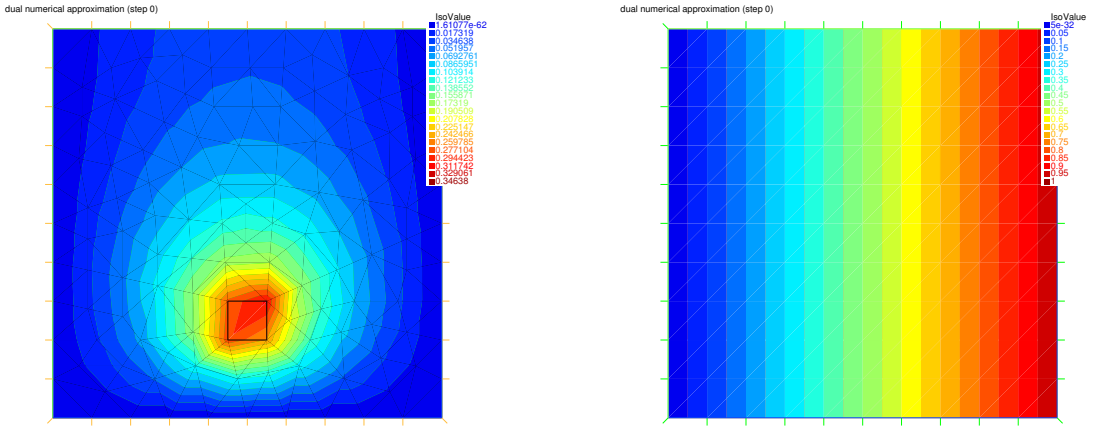

Figure 5: Approximate solution $\tilde{u}_\ell$ of the adjoint problem, $p = 1$ (left for Q_1 and right for Q_2)

2. The formula is still

$$\boldsymbol{\sigma}_\ell := \sum_{\boldsymbol{a} \in \mathcal{V}_\ell} \boldsymbol{\sigma}_\ell^{\boldsymbol{a}}, \tag{19a}$$

where

$$\boldsymbol{\sigma}_\ell^{\boldsymbol{a}} := \arg \min_{\substack{\boldsymbol{v}_\ell \in \mathcal{RT}_{p'}(\mathcal{T}_{\boldsymbol{a}}) \cap \boldsymbol{H}_0(\mathrm{div}, \omega_{\boldsymbol{a}}) \\ \nabla \cdot \boldsymbol{v}_\ell = \Pi_{p'}(f \psi^{\boldsymbol{a}} - \nabla u_\ell \cdot \nabla \psi^{\boldsymbol{a}})}} \| \psi^{\boldsymbol{a}} \nabla u_\ell + \boldsymbol{v}_\ell \|_{\omega_{\boldsymbol{a}}}^2. \tag{19b}$$

The space $\boldsymbol{H}_0(\mathrm{div}, \omega_{\boldsymbol{a}})$ for vertices $\boldsymbol{a}$ inside the computational domain Ω is the same as in tutorial N°1, i.e., the subspace of all functions from $\boldsymbol{H}(\mathrm{div}, \omega_{\boldsymbol{a}})$ whose normal trace vanishes on $\partial\omega_{\boldsymbol{a}}$. For a vertex $\boldsymbol{a}$ on the boundary of Ω, we request 1) the normal trace to vanish on the part of $\partial\omega_{\boldsymbol{a}}$ where $\psi^{\boldsymbol{a}}$ is zero (typically the part of $\partial\omega_{\boldsymbol{a}}$ not contained in $\partial\Omega$); 2) the normal trace to equal to $-\psi^{\boldsymbol{a}}$ on $\Gamma_\mathrm{N} \cap \partial\omega_{\boldsymbol{a}}$. Note that after summing in (19a), by virtue of the partition of unity $\sum_{\boldsymbol{a} \in \mathcal{V}_\ell} \psi^{\boldsymbol{a}} = 1$, the normal trace of the equilibrated flux $\boldsymbol{\sigma}_\ell$ on Γ_N is indeed equal to -1, in accordance with (1c).

4. Figure 6 shows the evolution of the goal estimates η_QI of (11) or (13) in comparison with the exact goal errors $|Q_j(u) - Q_j(u_\ell)|$. More specifically, we plot the effectivity indices given by (14) for both $j = 1$ and $j = 2$. We observe that they are perfectly close to the optimal value of one for Q_2 but rather increased for Q_1. The inspection of the primal and dual energy effectivity indices of (15) turns very much illuminating here. For the former one, in the case of Q_1, both are excellent, as witnessed in Figure 7. The reason why the bound (11) can be imprecise is a cornerstone of estimates in quantities of interest: both $\nabla(u - u_\ell)$ and $\nabla(\tilde{u} - \tilde{u}_\ell)$ can be nonzero vectors, but their scalar product can be (close to) zero, which harms the Cauchy–Schwarz bound in (11). In the case of Q_2, it follows from (18) that $\|\nabla(\tilde{u} - \tilde{u}_\ell)\| = \tilde{\eta}_\ell = 0$, so that we only see a consequence of rounding errors in the right part of Figure 8 (which explains the values below one), and only the two supplementary boundary terms in (13) form the estimate η_QI.

6. With the improved bound as defined by (17), we obtain the results of Figure 9. For Q_1, the effectivity indices are improved roughly by a factor of 2, whereas there is not much to improve for Q_2.

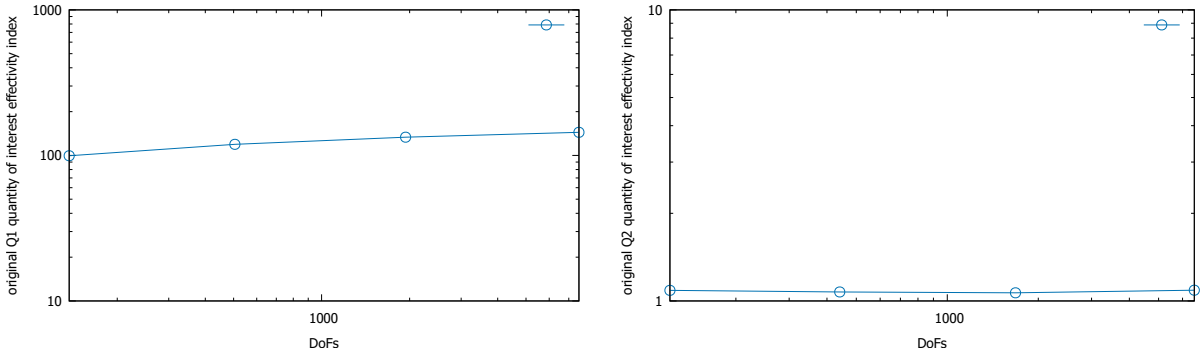

Figure 6: Quantity of interest effectivity indices (14), $p = 1$ (left for Q_1 and right for Q_2)

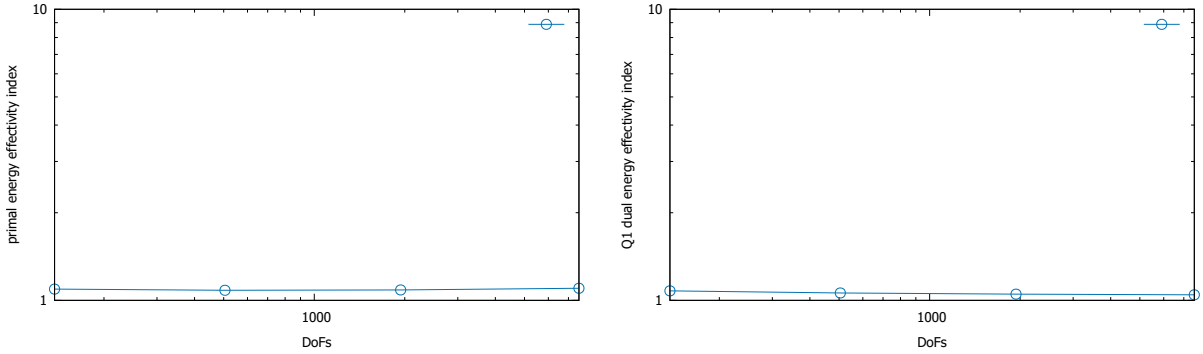

Figure 7: Energy error effectivity indices (15) for the primal (left) and dual (right) problems, $p = 1$ and Q_1

Exercise 3. (Mesh adaptation)

1. From the improved error estimate (17), in the case of Q_1, define the local error contributions as:

$$|Q_1(u) - Q_1(u_\ell)| \leq \eta_{\mathrm{QI}}^{\mathrm{impr}} := \max_{\theta=\pm 1} \left| \sum_{K \in \mathcal{T}_\ell} C_\ell^K + \frac{\theta}{2} \sqrt{\sum_{K \in \mathcal{T}_\ell} \xi_K^2} \right| \tag{20a}$$

   where for all $K \in \mathcal{T}_\ell$, C_ℓ^K is the local contribution to C_ℓ, i.e.

$$C_\ell^K := \frac{1}{2}(\boldsymbol{\sigma}_\ell + \nabla u_\ell, \tilde{\boldsymbol{\sigma}}_\ell + \nabla \tilde{u}_\ell)_K, \tag{20b}$$

   and

$$\xi_K^2 = \frac{1}{2}(\eta_\ell^2 \tilde{\eta}_K^2 + \eta_K^2 \tilde{\eta}_\ell^2). \tag{20c}$$

2. Adapt the mesh following these elementwise error estimators. Please report all the distribution of ξ_K, C_ℓ^K, the primal and dual energy errors $\|\nabla(u - u_\ell)\|_K$, $\|\nabla(\tilde{u} - \tilde{u}_\ell)\|_K$, the primal and dual energy estimators $\|\boldsymbol{\sigma}_\ell + \nabla u_\ell\|_K$, $\|\tilde{\boldsymbol{\sigma}}_\ell + \nabla \tilde{u}_\ell\|_K$, and the sequence of refined meshes. Compare the results to those of uniform mesh refinement of Exercises 1 and 2.

Answer 3. (Mesh adaptation)

The answer to item 1 is contained in the script `TP3.edp`.

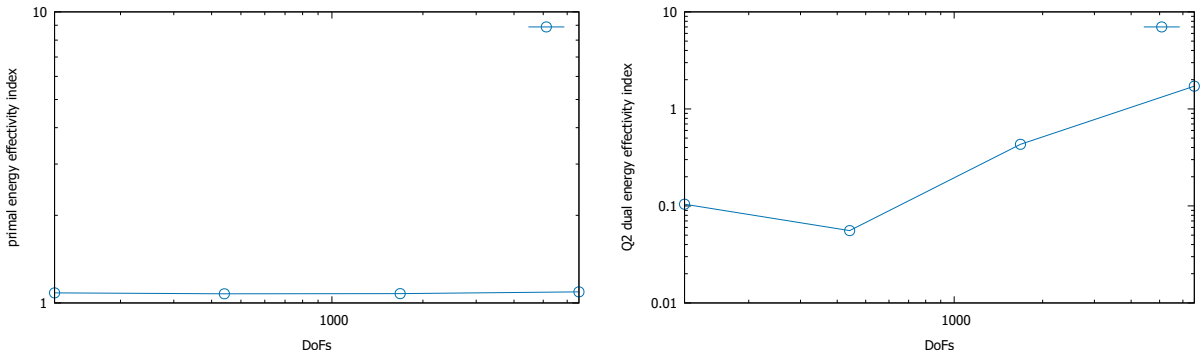

Figure 8: Energy error effectivity indices (15) for the primal (left) and dual (right) problems, $p = 1$ and Q_2

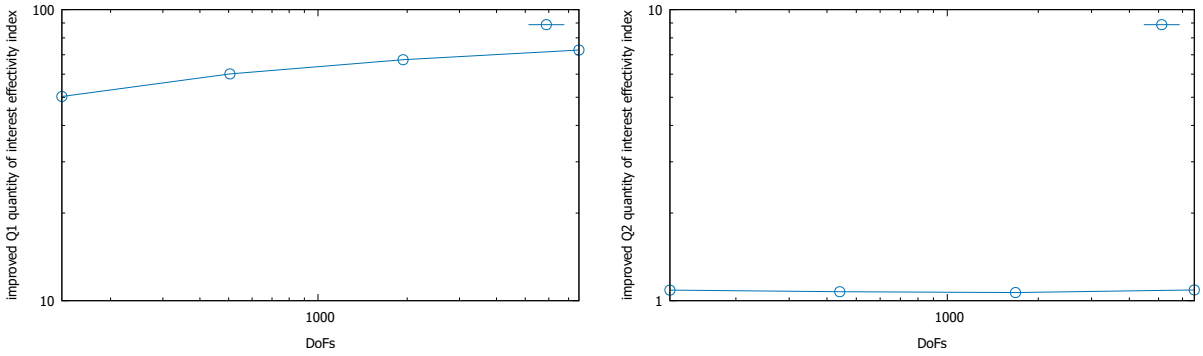

Figure 9: Effectivity indices given by the ratio $\eta_{\mathrm{QI}}^{\mathrm{impr}}/|Q_j(u) - Q_j(u_\ell)|$ of the improved goal error estimate over the exact goal error, see (17), $p = 1$ (left for Q_1 and right for Q_2)

2. The results are given in Figures 10–14. We see a good prediction of the localization of both the primal and dual energy errors. Then, refinement based on the combined estimator ξ_K adjusts the meshes towards all the problematic areas – the two upper corners and the vicinity of ω_Q. Figure 14, however, shows that the evolution of the quantity of interest error $|Q_1(u) - Q_1(u_\ell)|$ with respect to the number of DoFs, with mesh adaptation, does not improve considerably over uniform meshes. The reason is that the best-possible error decay has already been achieved with uniform mesh refinement, see Figure 4. The effectivity indices, though, improve well in comparison with uniform mesh refinement, see Figure 9, left.

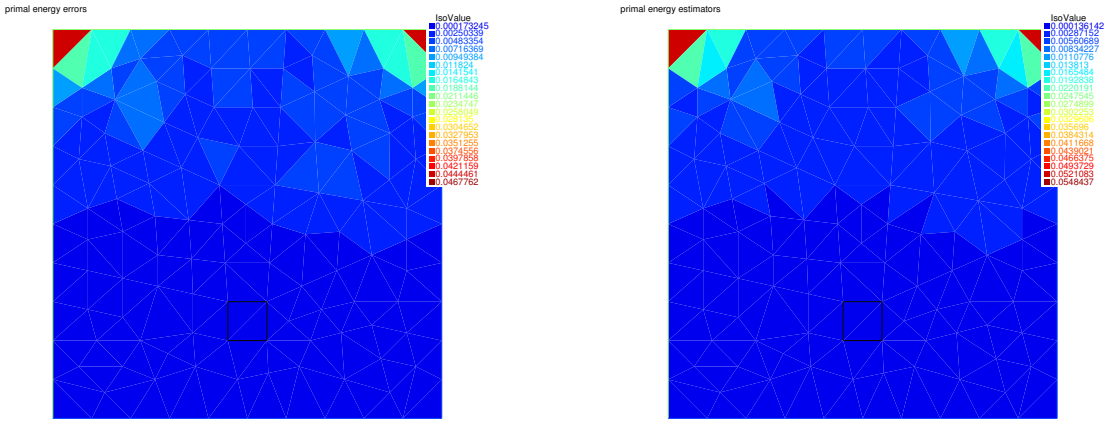

Figure 10: Primal energy errors $\|\nabla(u-u_\ell)\|_K$ (left) and primal energy estimators $\|\boldsymbol{\sigma}_\ell + \nabla u_\ell\|_K$ (right), $p=1$, Q_1

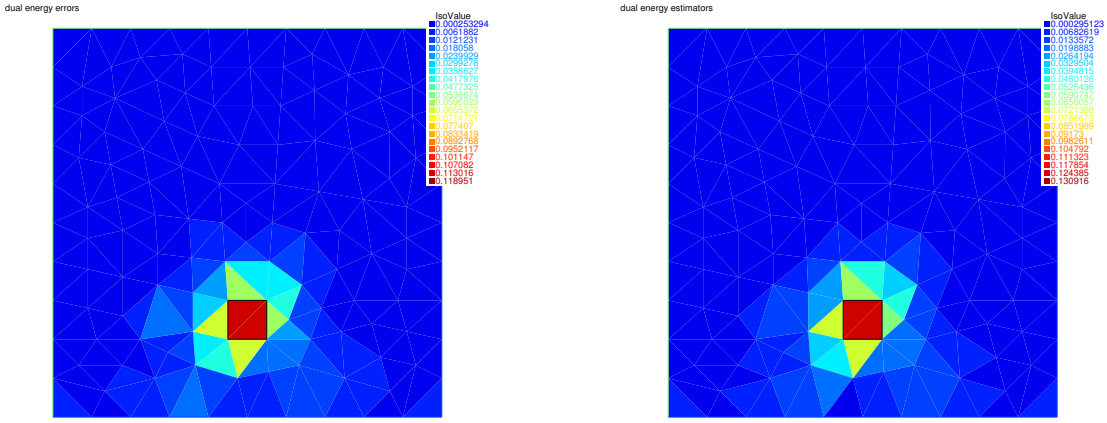

Figure 11: Dual energy errors $\|\nabla(\tilde{u}-\tilde{u}_\ell)\|_K$ (left) and dual energy estimators $\|\tilde{\boldsymbol{\sigma}}_\ell+\nabla\tilde{u}_\ell\|_K$ (right), $p=1$, Q_1

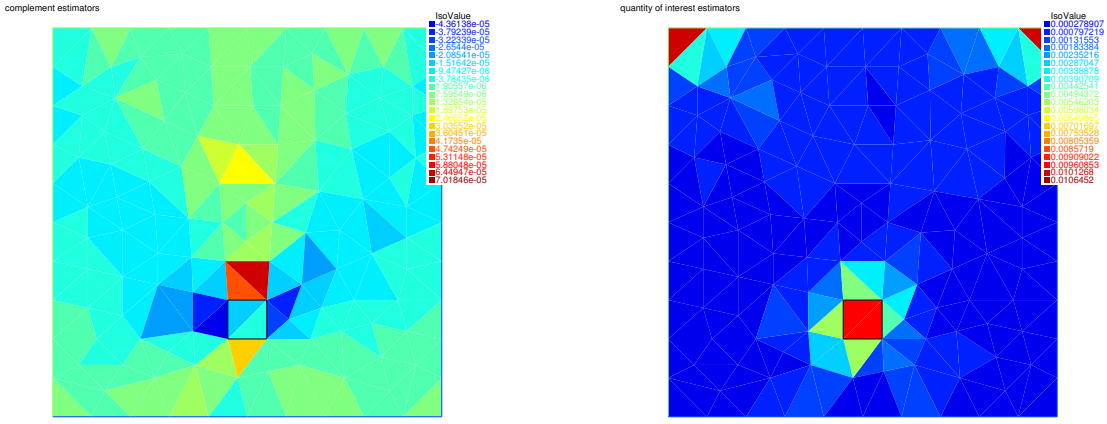

Figure 12: The correction estimators C_ℓ^K from (20b) (left) and the quantity of interest estimators ξ_K from (20c) (right), $p=1$, Q_1

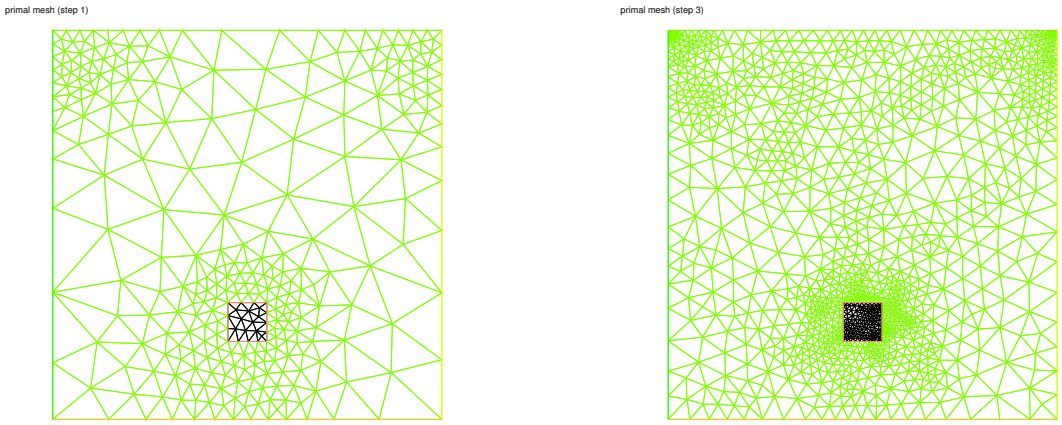

Figure 13: The first (left) and fourth (right) adapted mesh, $p = 1$, Q_1

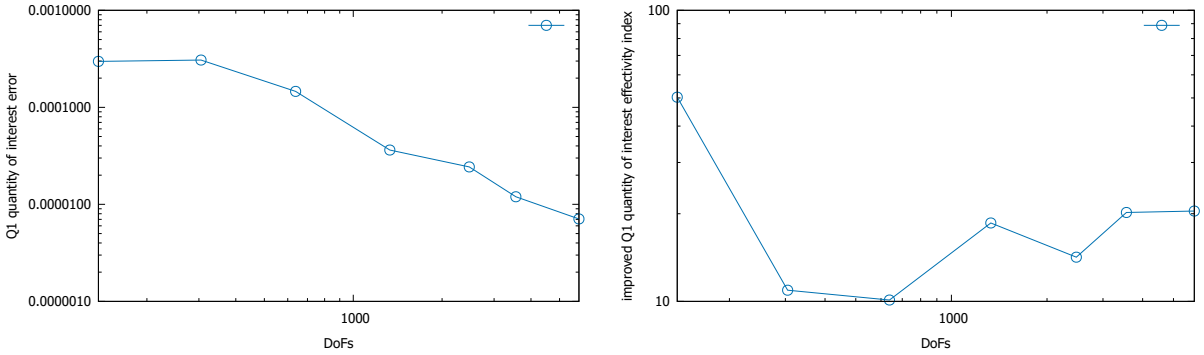

Figure 14: The quantity of interest errors $|Q_1(u) - Q_1(u_\ell)|$ with respect to the DoFs (left) and the improved goal effectivity indices (17) (right), mesh adaptation, $p = 1$, Q_1

Exercise 4. (Alternative strategy for adaptivity)

One may think of a strategy where the mesh for the adjoint problem alone is refined, following the estimator $\|\tilde{\boldsymbol{\sigma}}_\ell + \nabla \tilde{u}_\ell\|_K$ (this might be expected to happen in the vicinity of the adjoint loading where the changes in the local gradients are high), while keeping the mesh of the primal problem unchanged. Denoting $\tilde{u}_{\bar{\ell}}$ the associated adjoint finite element approximation and $\tilde{\boldsymbol{\sigma}}_{\bar{\ell}}$ the corresponding equilibrated flux, the a posteriori error bound now reads, for Q_1,

$$|Q_1(u) - Q_1(u_\ell)| \leq \eta_{\mathrm{QI}} := \eta_\ell \tilde{\eta}_{\bar{\ell}}. \tag{21}$$

Taking $C_{\bar{\ell}} := \frac{1}{2}(\boldsymbol{\sigma}_\ell + \nabla u_\ell, \tilde{\boldsymbol{\sigma}}_{\bar{\ell}} + \nabla \tilde{u}_{\bar{\ell}})$ and $\tilde{\eta}_{\bar{\ell}} := \|\tilde{\boldsymbol{\sigma}}_{\bar{\ell}} + \nabla \tilde{u}_{\bar{\ell}}\|$, we also have

$$|Q_1(u) - Q_1(u_\ell) - C_{\bar{\ell}}| \leq \frac{1}{2}\eta_\ell \tilde{\eta}_{\bar{\ell}}$$

and consequently

$$|Q_1(u) - Q_1(u_\ell)| \leq \eta_{\mathrm{QI}}^{\mathrm{impr}} := \max_{\theta=\pm 1} \left| C_\ell + \frac{\theta}{2}\eta_\ell \tilde{\eta}_\ell \right|. \tag{22}$$

1. For a sequence of locally adapted meshes when solving the adjoint problem but a fixed mesh for the primal problem, analyze the evolution of the goal estimate with respect to the exact goal error, and plot effectivity indices.

Answer 4. (Alternative strategy for adaptivity)

1. Setting `bool MeshRefAdjoint = true` allows to perform the simulations and Figure 15 shows the results. Since the primal mesh $\mathcal{T}_0$ does not change, $|Q_1(u) - Q_1(u_\ell)|$, as well as $\|\boldsymbol{\sigma}_\ell + \nabla u_\ell\|$ (for $\ell = 0$), are constant. The quality of the dual error estimate $\|\nabla(\tilde{u} - \tilde{u}_{\bar{\ell}})\| \leq \tilde{\eta}_{\bar{\ell}} := \|\tilde{\boldsymbol{\sigma}}_{\bar{\ell}} + \nabla \tilde{u}_{\bar{\ell}}\|$, in turn, improves. Thus the effectivity indices for the quantity of interest improve.

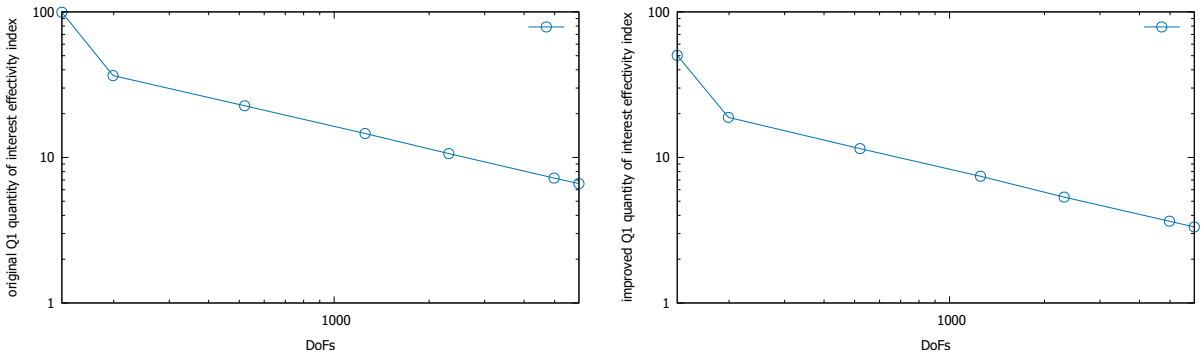

Figure 15: Quantity of interest effectivity indices given by the ratio $\eta_{\mathrm{QI}}/|Q_1(u) - Q_1(u_\ell)|$ from (21) (left) and $\eta_{\mathrm{QI}}^{\mathrm{impr}}/|Q_1(u) - Q_1(u_\ell)|$ from (22) (right), $p = 1$, Q_1

Exercise 5. (Goal-oriented error estimation near singularities)

We now consider a domain with a square hole of size 0.2×0.2 centered at point $(0.5, 0.5)$, see Figure 16. Consequently, the solutions will exhibit local singularities. The same boundary conditions as in the previous example are applied on the external boundary, while a free edge condition $-\nabla u \cdot \boldsymbol{n}_\Omega = 0$ is considered on the border Γ_S of the hole.

1. Perform the same analysis as before, considering as the quantity of interests again

$$Q_1(u) := \frac{1}{|\omega_Q|} \int_{\omega_Q} u \quad \text{and} \quad Q_2(u) := -\frac{1}{|\Gamma_R|} \int_{\Gamma_R} \frac{\partial u}{\partial x};$$

in the first case, the subregion $\omega_Q := (0.45, 0.55) \times (0.2, 0.3)$ can be potentially moved closer to the singularity. For this example, a reference solution needs to be computed from an overkill mesh.

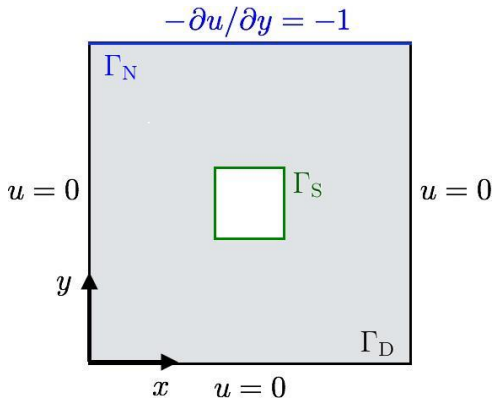

Figure 16: New reference problem

Answer 5. (Goal-oriented error estimation near singularities)

The corresponding code is contained in the script `TP3.edp` and evoked using the setting `bool hole = true`. We now present the answers to Exercises 1–4.

Exercise 1: Analysis of the error

4. Figure 17 shows the exact solution u and its finite element approximation u_ℓ on the new domain with the hole.

5. Figure 18 depicts the convergence of the primal energy error $\|\nabla(u - u_\ell)\|$. The errors in the quantities of interest $|Q_j(u) - Q_j(u_\ell)|$ are then reported in Figure 19. We obtain the rate 0.43 for the primal energy error and 0.67 for the error in the Q_1 quantity of interest. For the Q_2 quantity of interest, the rate appears to be bigger than 1 here; it seems that a rather precise approximation of the unknown exact solution u is necessary (we take `noverkill = 2` and `Pcontpp P4`).

Exercise 2: Goal-oriented error estimation

1. One should obtain the results of Figure 20.

4. Figure 21 shows the quantity of interest effectivity indices (14). The values slightly below 1 for Q_2 seem to originate in a still not enough precise approximation of the unknown exact solution u. The energy error effectivity indices reported in Figures 22 and 23 seem, in turn, excellent.

6. With the improved bound as defined by (17), we obtain the results of Figure 24.

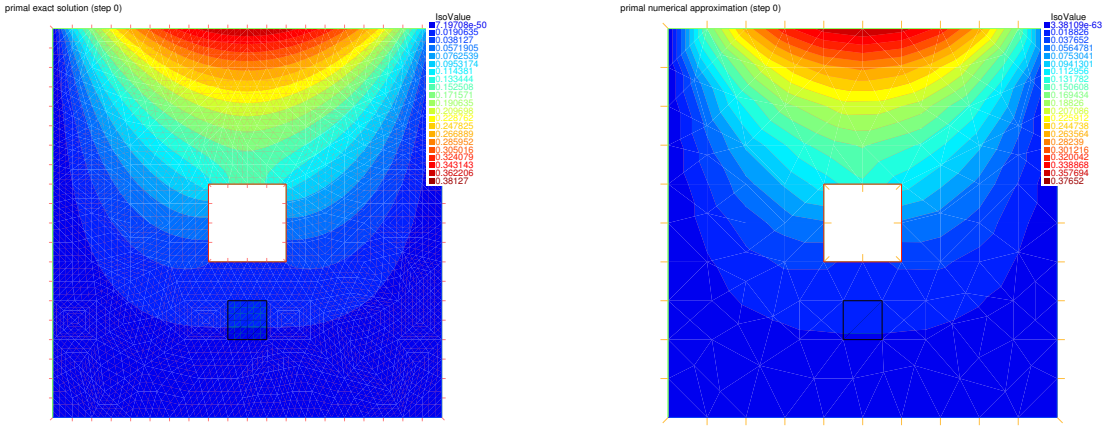

Figure 17: Exact solution u (left) and approximate solution u_ℓ (right, $p = 1$), domain with hole of Figure 16

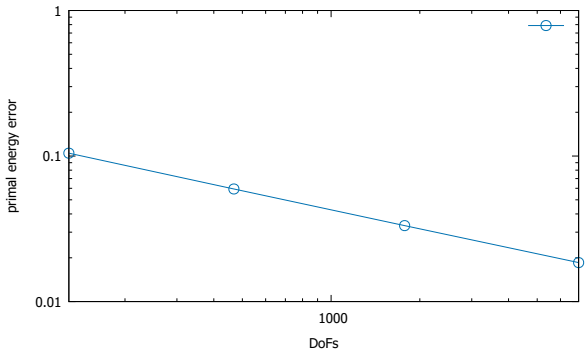

Figure 18: Energy error $\|\nabla(u - u_\ell)\|$ with respect to the DoFs, $p = 1$, domain with hole of Figure 16

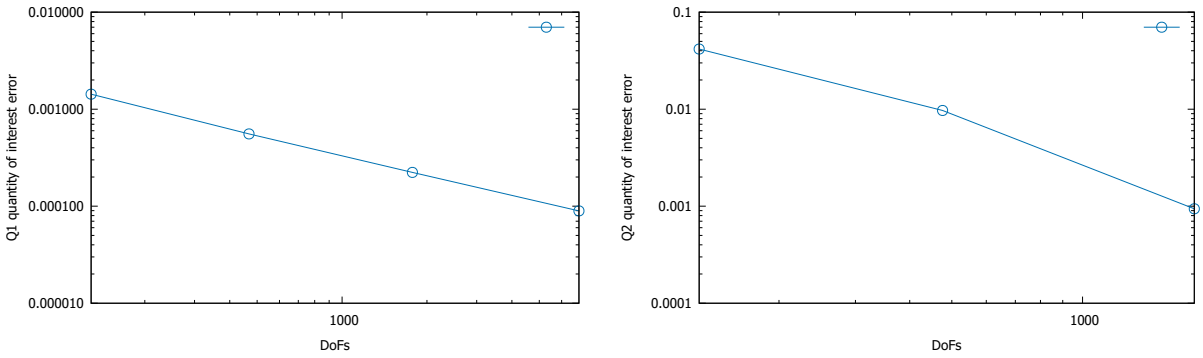

Figure 19: Error in the quantity of interest $|Q_j(u) - Q_j(u_\ell)|$ in function of the DoFs, $p = 1$ (left for Q_1, right for Q_2), domain with hole of Figure 16

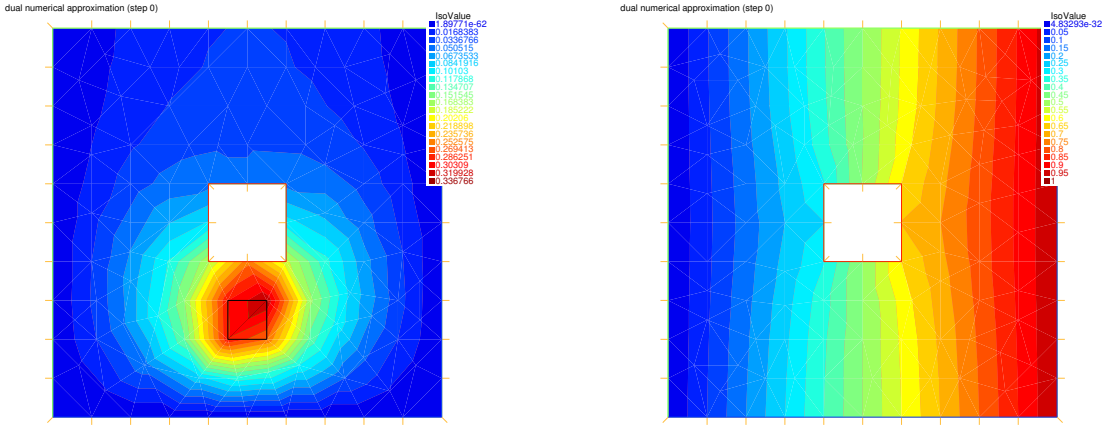

Figure 20: Approximate solution $\tilde{u}_\ell$ of the adjoint problem, $p = 1$ (left for Q_1 and right for Q_2), domain with hole of Figure 16

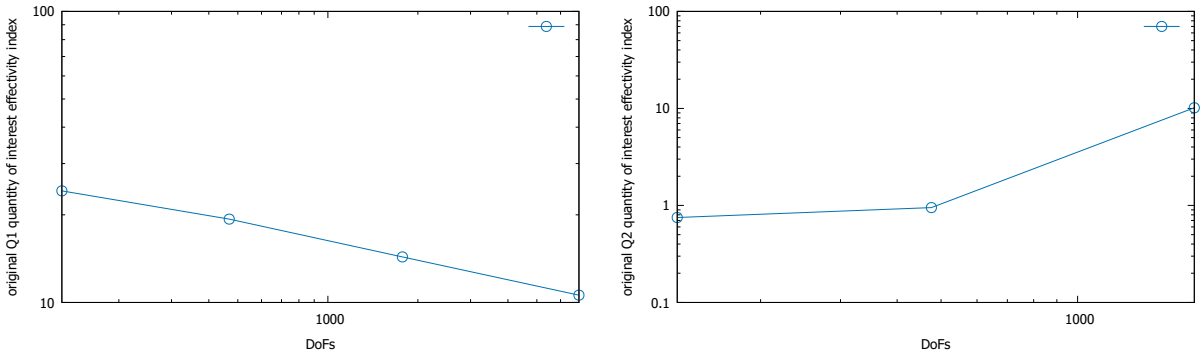

Figure 21: Quantity of interest effectivity indices (14), $p = 1$ (left for Q_1 and right for Q_2), domain with hole of Figure 16

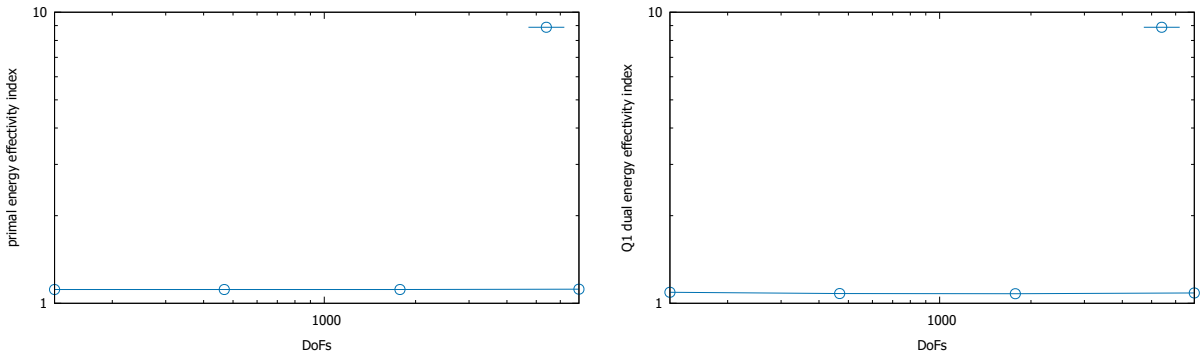

Figure 22: Energy error effectivity indices (15) for the primal (left) and dual (right) problems, $p = 1$ and Q_1, domain with hole of Figure 16

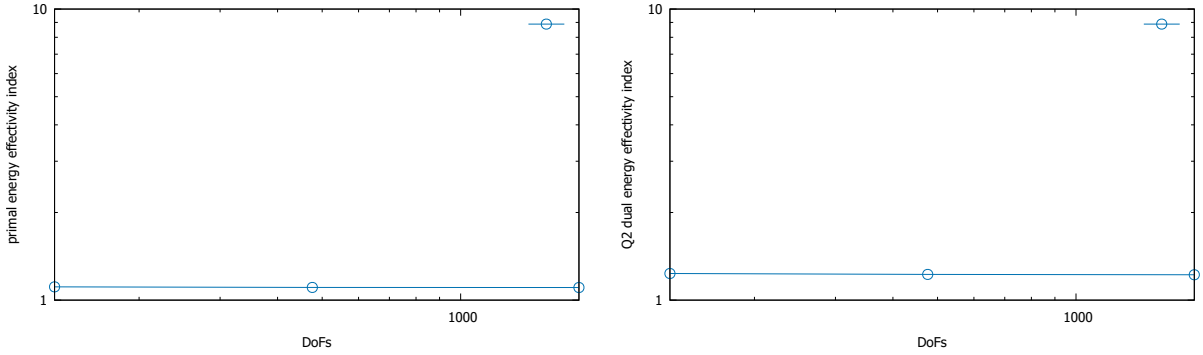

Figure 23: Energy error effectivity indices (15) for the primal (left) and dual (right) problems, $p = 1$ and Q_2, domain with hole of Figure 16

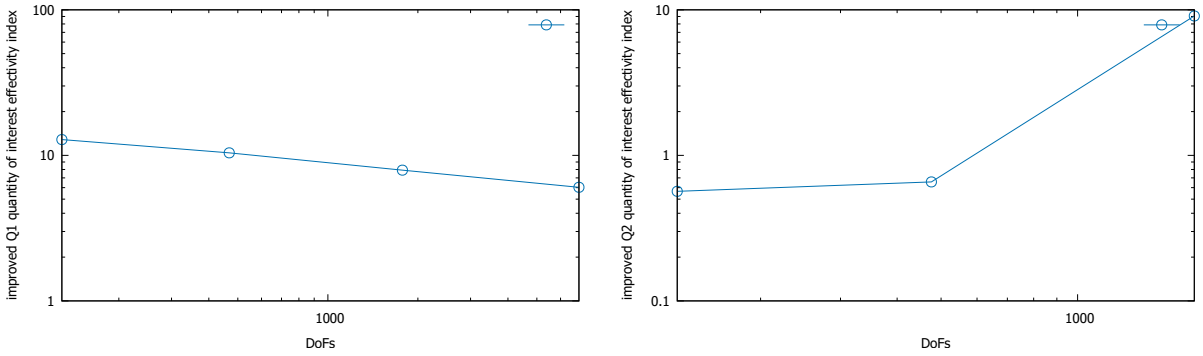

Figure 24: Effectivity indices given by the ratio $\eta_{\mathrm{QI}}^{\mathrm{impr}}/|Q_j(u) - Q_j(u_\ell)|$ of the improved goal error estimate over the exact goal error, see (17), $p = 1$ (left for Q_1 and right for Q_2), domain with hole of Figure 16

Exercise 3: Mesh adaptation

2. The results are given in Figures 25–29. We again observe a good prediction of the localization of both the primal and dual energy errors. In comparison with Exercise 3, four strong singularities appear around the four re-entrant corners of the hole. Then, refinement based on the combined estimator ξ_K adjusts the meshes towards all the problematic areas. In Figure 29, we see that the evolution of the quantity of interest error $|Q_1(u) - Q_1(u_\ell)|$ with respect to the number of DoFs, with mesh adaptation, is now significantly improved over uniform meshes, approaching the optimal rate of 1.

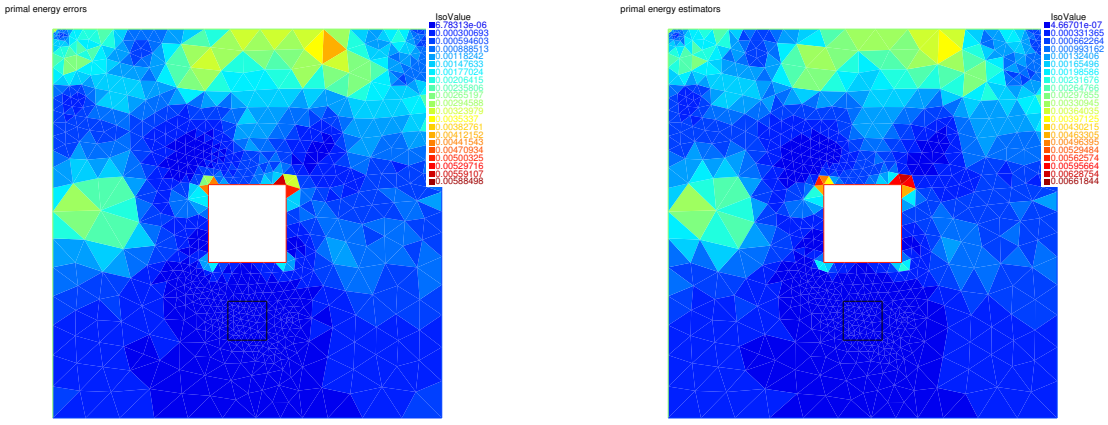

Figure 25: Primal energy errors $\|\nabla(u - u_\ell)\|_K$ (left) and primal energy estimators $\|\boldsymbol{\sigma}_\ell + \nabla u_\ell\|_K$ (right), $p = 1$, Q_1, domain with hole of Figure 16

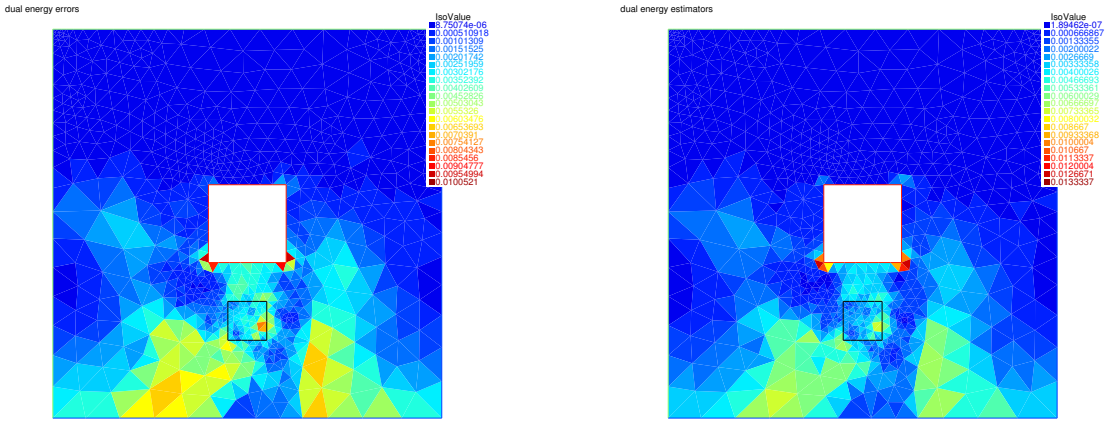

Figure 26: Dual energy errors $\|\nabla(\tilde{u} - \tilde{u}_\ell)\|_K$ (left) and dual energy estimators $\|\tilde{\boldsymbol{\sigma}}_\ell + \nabla\tilde{u}_\ell\|_K$ (right), $p = 1$, Q_1, domain with hole of Figure 16

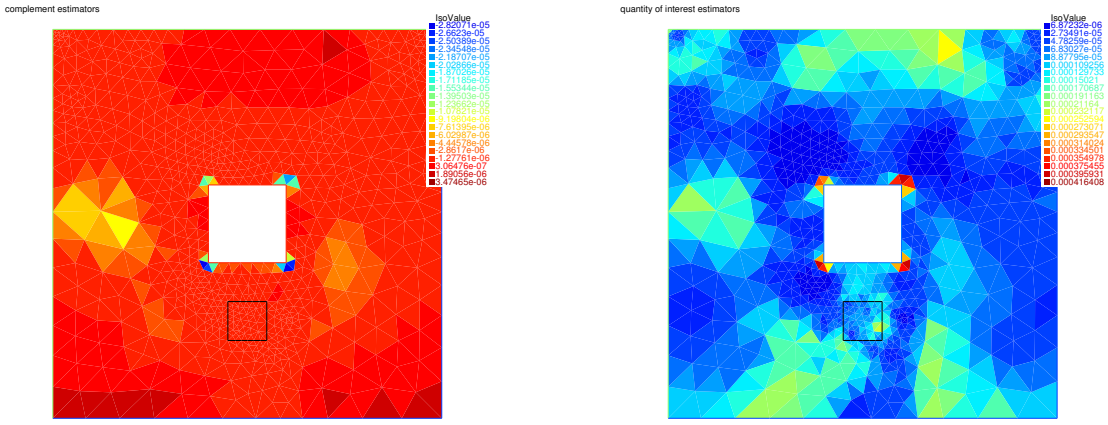

Figure 27: The correction estimators C_ℓ^K from (20b) (left) and the quantity of interest estimators ξ_K from (20c) (right), $p = 1$, Q_1, domain with hole of Figure 16

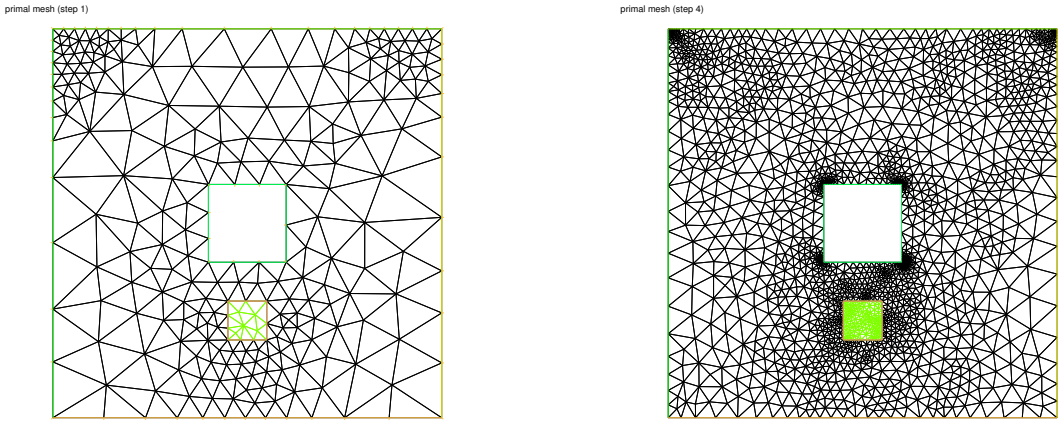

Figure 28: The first (left) and fourth (right) adapted mesh, $p = 1$, Q_1, domain with hole of Figure 16

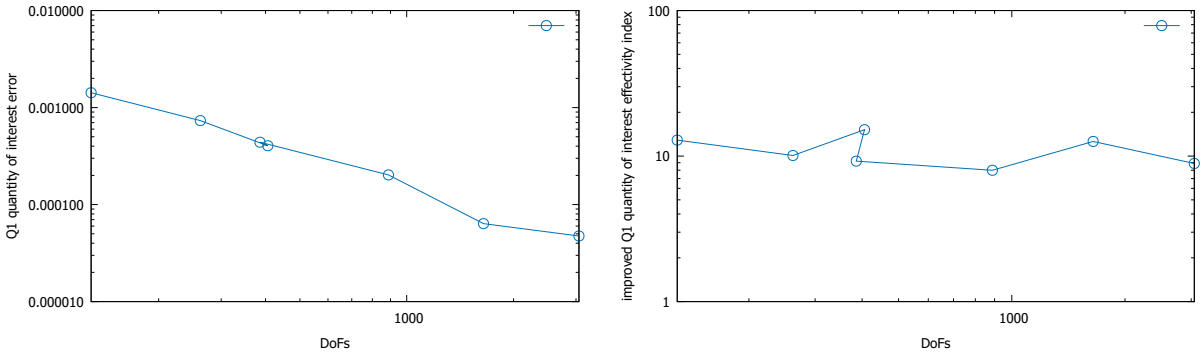

Figure 29: The quantity of interest errors $|Q_1(u) - Q_1(u_\ell)|$ with respect to the DoFs (left) and the improved goal effectivity indices (17) (right), mesh adaptation, $p = 1$, Q_1, domain with hole of Figure 16

References

[1] Mallik, G., Vohralík, M., and Yousef, S. Goal-oriented a posteriori error estimation for conforming and nonconforming approximations with inexact solvers. *J. Comput. Appl. Math. 366* (2020), 112367.